PAPER

Magnetism and variable temperature and pressure crystal structures of a linear oligonuclear cobalt bis-semiquinonate†

Jacob Overgaard,*[a] Louise H. Møller,[a] Mette A. Borup,[a] Maxime Tricoire,[a] James P. S. Walsh,[b] Marcel Diehl[c,d] and Eva Rentschler*[c]

The crystal structure of the first oligomeric cobalt dioxolene complex, $Co_3(3,5\text{-DBSQ})_2(^tBuCOO)_4(NEt_3)_2$, **1**, where DBSQ is 3,5-di-*tert*-butyl-semiquinonate, has been studied at various temperatures between 20 and 200 K. Despite cobalt–dioxolene complexes being generally known for their extensive ability to exhibit valence tautomerism (VT), we show here that the molecular geometry of compound **1** is essentially unchanged over the full temperature range, indicating the complete absence of electron transfer between ligand and metal. Magnetic susceptibility measurements clearly support the lack of VT between 8 and 300 K. The crystal structure is also determined at elevated pressures in the range from 0 to 2.5 GPa. The response of the crystal structure is surprisingly dependent on the dynamics of pressurisation: following rapid pressurization to 2 GPa, a structural phase transition occurs; yet, this is absent when the pressure is increased incrementally to 2.6 GPa. In the new high pressure phase, Z′ is 2 and one of the two molecules displays changes in the coordination of one bridging carboxylate from $\mu_2:\kappa O:\kappa O'$ to $\mu_2:\kappa^2 O,O':\kappa O'$, while the other molecule remains unchanged. Despite the significant changes to the molecular connectivity, analysis of the crystal structures shows that the phase transition leaves the spin and oxidation states of the molecules unaltered. Intermolecular interactions in the high pressure crystal structures have been analysed using Hirshfeld surfaces but they cannot explain the origin of the phase transition. The lack of VT in this first oligomeric Co-dioxolene complex is speculated to be due to the coordination geometry of the terminal Co-atoms, which are trigonal bipyramidally coordinated, different from the more common octahedral coordination. The energy that is gained by a *hs*-to-*ls* change in O_h is equal to Δ, while in the case of the trigonal bipyramidal (C_{3v}), the energy gain is equal to the splitting between $d(z^2)$ and degenerate $d(x^2 - y^2)/d(xy)$, which is significantly less.

Introduction

Valence tautomerism (VT) is a phenomenon with various potential applications, most notably as miniature switches.[1–5] Cobalt coordination complexes that contain one or two molecules belonging to the non-innocent ligand group *cis*-dioxolenes (diox) are particularly well-studied in this context since they possess a combination of structural and electronic features that favour the VT mechanism to occur at moderately high temperatures.[6–9]

The VT transition involves a metal-to-ligand charge transfer and an accompanying change in the spin-value of the metal. Above the transition temperature, the electronic configuration is typically described as a high-spin d^7 Co(II) with a monoanionic semiquinone (sq) radical. Upon cooling, the system undergoes a transition into a state described as a low-spin d^6 Co(III) with a di-anionic, diamagnetic catecholate (cat). The changes induced upon going from a paramagnetic to a diamagnetic regime make these two molecular states markedly different.

The VT transition is known to be triggered by: (i) temperature; (ii) electromagnetic irradiation (visible light or X-rays); (iii) pressure; and (iv) magnetic/electric fields. Temperature-induced VT is driven by entropy; the *hs*-Co(II)-SQ state has a higher density of vibrational states due to its longer Co–ligand separations and higher spin multiplicity. Thus, higher

[a]Department of Chemistry, Aarhus University, Langelandsgade 140, 8000 Aarhus C, Denmark. E-mail: jacobo@chem.au.dk
[b]Department of Chemistry, Northwestern University, Evanston, IL 60208, USA
[c]Institute of Inorganic and Analytical Chemistry, Johannes Gutenberg University Mainz, D-55128 Mainz, Germany
[d]Graduate School Materials Science in Mainz, Staudingerweg 9, D-55128 Mainz, Germany
†Electronic supplementary information (ESI) available. CCDC 1481083–1481098. For ESI and crystallographic data in CIF or other electronic format see DOI: 10.1039/c6dt02024k

temperatures favour the *hs*-state, which may convert into the *ls*-Co(III)-cat state upon cooling.[2,3,7–13]

Light-induced VT involves excitations in either the metal-to-ligand charge-transfer (MLCT) band or in the ligand-to-metal charge-transfer (LMCT) band. The latter is typically employed to revert the VT transition that follows from a lowering of the temperature. The photo-induced excited states are metastable, and are found to survive only at temperatures below roughly 50 K.[14–16] However, not only using visible light can VT be induced, but also soft X-rays were shown to lead to MLCT. This effect was attributed to inelastic scattering of secondary electrons with the same energy as the ligand to metal charge transfer (LMCT) transition thus being able to induce VT transition.[17]

Pressure-induced VT is a transition from the high-spin to the low-spin state upon increasing applied pressure. This can be explained by the fact that the *ls*-Co(III)-cat state exhibits significantly shorter Co–ligand bond distances, and is thus the more stable form at higher pressures.[18–21] Besides external pressure, chemically pressure induced by ligand constraints or solvents being present in the crystal lattice is also possible.[22,23]

Other interesting effects have been reported recently, such as VT transition triggered by the application of strong magnetic fields, or the theoretically predicted VT upon application of an electric field.[24,25]

Historically, the research on VT in cobalt–dioxolene complexes has focused on three main classes: [Co(diox)(N$_4$L)]$^+$, [Co(sq)(diox)(N$_2$L)], and trans-[Co(sq)(diox)(NL)$_2$], where N$_x$L is a tetra-, bi-, or monodentate nitrogen donor ancillary ligand, respectively. Studies involving systematic changes to the nitrogen donor ancillary ligands have led to some important conclusions.[22] It is observed that the transition temperature, $T_{1/2}$, can be controlled by the electron withdrawing capability of the chosen substituents. An increased electron withdrawal leads to a decrease in the ligand donor strength and stabilisation of the softer of the two possible Co-states (*i.e.* the *hs*-Co(II) form) and thus a dramatic change in the transition temperature.[22,26,27] The value of $T_{1/2}$ can also be tuned by varying the chelate ring flexibility of the nitrogen-based co-ligands. Bigger chelate ring sizes result in entropic stabilisation of the *hs*-Co(II) redox isomer and hence lead to a decrease in $T_{1/2}$. Cooperative effects can also lead to hysteresis in the VT transition, and have been found to stabilise photo-induced metastable states.[23,28–30]

In dinuclear spin-crossover (SCO) complexes, intramolecular cooperativity leads to three distinct spin states (*ls–ls*, *ls–hs* and *hs–hs*) exhibiting hysteresis in their transitions, which makes them interesting as potential three-state switches or molecular ternary memory components.[31,32] Given the similarities of the SCO and VT phenomena, it is warranted to expect the same properties for VT complexes containing multiple metal centres. Several synthetic strategies have been employed to isolate dinuclear VT complexes, with the most prominent member of the family having the general formula [(Co(sq)(diox))$_2$(N$_2$LN$_2$)], where N$_2$LN$_2$ is a bridging bis-bidentate nitrogen donor ancillary ligand such as bis(diimine).[33–35]
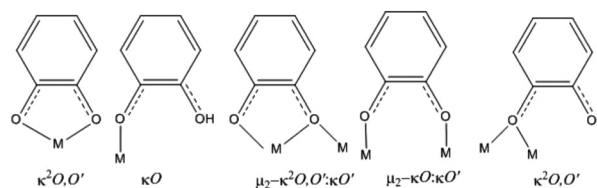
Scheme 1 Possible coordination modes of dioxolene ligands.

Other examples of dinuclear cobalt complexes showing VT include the use of ligands derived from 2,5-dihydroxy-1,4-benzoquinone (dhbq) as bridging moieties. Complexes that reveal both thermally as well as photoinduced VT for one of the cobalt centers have been reported.[12,36–38]

As for the dinuclear dioxolene complexes, two general strategies for the synthesis of polynuclear VT complexes are found in the literature: employing either a bridging nitrogen donor ligand (NLN)[10,39–41] or the redox-active ligand itself (diox-R-diox) as bridging moiety.[42–46]

While for most dioxolene complexes the ligands coordinate as bidentate chelates with both oxygen donor atoms bound to the same metal ion, a number of other coordination modes are found in oligomeric complexes (see Scheme 1). Besides the simple monodentate coordination of a protonated ligand, or the bridging, non-chelating μ_2-κO:κO′ fashion, the μ_2 bridging coordination in a chelating μ_2-κ^2O,O′:κO′ mode is most common in such oligomeric compounds.[47–51]

In the present study we describe the first successful synthesis of a Co-dioxolene complex in which the metal chain has been elongated to include three Co-atoms in a single discrete molecule. Moreover, to the best of our knowledge, this is the first linear oligonuclear Co-dioxolene compound showing exclusively the coordination mode μ^2-κ^1:κ^1. The formation of the oligonuclear compound has been encouraged by the use of coordinative unsaturated cobalt carboxylate as starting material. It is generally not possible to predict *ab initio* whether a given compound exhibits temperature-dependent VT; however, the combined electron-donating or withdrawing abilities of the coordinated ligands are important factors to consider, since they influence the ease with which the charge transfer can occur. In this study we have monitored the VT using both multi-temperature single crystal diffraction as well as variable-temperature magnetic susceptibility.

Results and discussion

Molecular structure

Compound **1** crystallises in space group $P\bar{1}$ with the entire molecule in the asymmetric unit. The molecular structure of **1** is shown in Fig. 1 with only the most occupied atoms of the disordered parts included. In one end of the molecule, there is significant positional disorder, which affects Co3 and the NEt$_3$ group bonded to it, as well as two of the four *tert*-butyl groups of the pivalate bridges. The disorder has been modelled as two
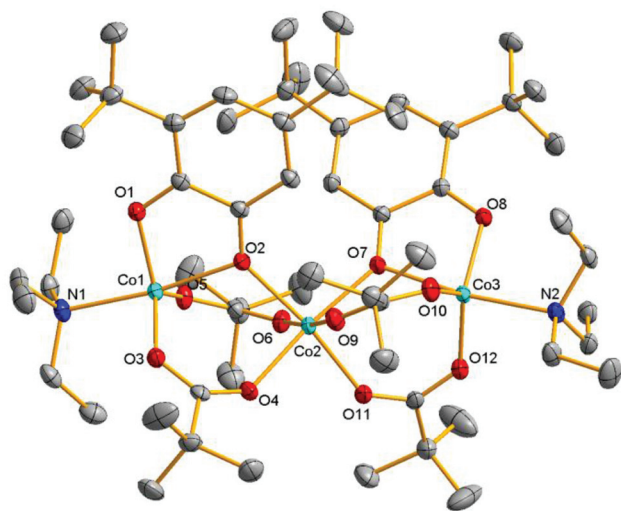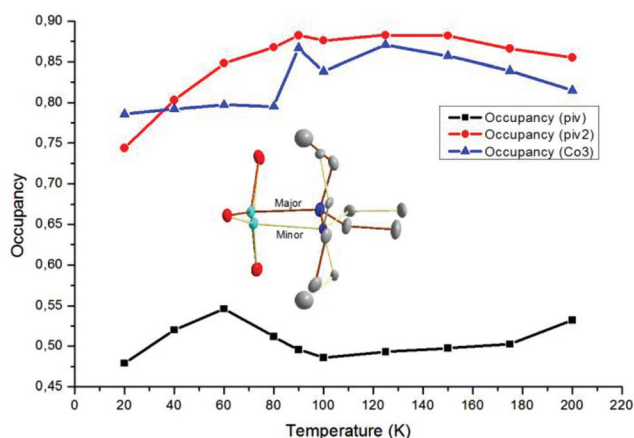
Fig. 1 ORTEP drawing of **1**, showing only the major occupancies of the disordered parts, and with hydrogen atoms omitted for clarity. The thermal ellipsoids are shown at the 50% probability level. The program Diamond has been used to prepare the graphics.

independent positions of the involved atoms (see inset in Fig. 2).

The evolution of the positional disorder in the two *tert*-butyl and terminal Co3 parts as a function of temperature is shown in Fig. 2. The lack of any significant slope shows that the disorder is essentially independent of temperature. It is unclear whether the apparent correlation between the disorder on the Co–NEt$_3$ moiety and the *t*-butyl part of the μ$_2$-bridging pivalato group linking Co1 and Co2 (here denoted piv2) is accidental or not. At 100 K, a high-resolution data set was collected with the intention of performing charge density modelling.[52] However, this proved impossible due to the severe disorder. Trimming this high resolution data set at different resolution reveals that the degree of disorder is not influenced by the
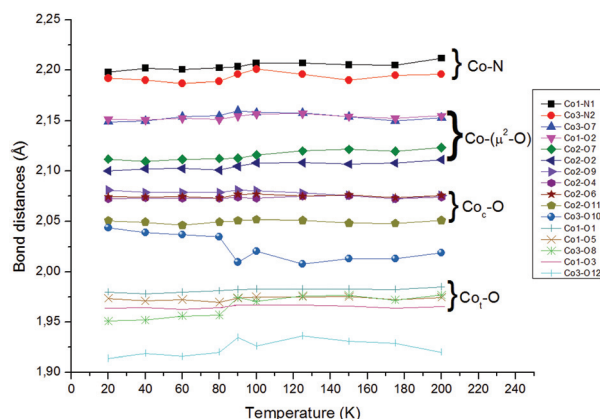
data-resolution. Testing different crystals indicate that the behaviour is sample-dependent.

The temperature dependence of the central Co–ligand bond distances is illustrated in Fig. 3. The different bond types group together nicely, with the exception of two bonds involving Co3. This discrepancy stems from the disorder of that particular part of the molecule, which has a strong influence on the precision of the atomic positions of both the Co atom and the surrounding ligands. Overall, it is clear that bond distances are unaffected by temperature in compound **1**, in contrast to the situation that would be observed if the system exhibited a VT transition in the given temperature range. Thus, we can unambiguously rule out the presence of VT in this temperature interval. Furthermore, the values of the bond lengths clearly support the presence of a *hs*-Co(II) system, particularly for the central pseudo-octahedrally coordinated Co2.

A search in the Cambridge Structural Database (CSD version 5.37) for molecules containing a six-coordinate Co atom bonded to one 3,5-DBSQ, or the related benzoquinone or catecholate, as well as four additional oxygen or nitrogen atoms, results in a bimodal distribution of bond distances (Fig. S1†). The majority of the distances found in the search represent shorter Co–O bond lengths (average d(Co–O) = 1.883 Å), corresponding to low-spin Co(III), with a smaller number representing longer bond lengths (average d(Co–O) = 2.051 Å), corresponding to high-spin Co(II). We find here values in the range 2.05–2.12 Å for the six-coordinate central Co2, matching the few long bond distances found in the CSD (Fig. S1†) and thus we assign it as high-spin Co(II).

The situation is less clear-cut for the five-coordinate terminal Co-atoms (Co1 and Co3) due to the presence of static disorder on the Co3 position, which invariably increases the uncertainty for the refined positions and hence bond distances in that end of the molecule. Therefore, the subsequent analysis has only been carried out using the geometry around Co1. The coordination sphere of Co1 is distorted trigonal bipyramidal, and the combination of a Co-DBSQ complex in that particular geometry occurs only very rarely in the CSD (six structures fulfil the criteria, see ESI†). However, it fits perfectly

Fig. 2 Occupancy of the major part of the three disordered moieties, the two pivalate groups and the Net$_3$ group, plotted as a function of temperature. The inset illustrates the disorder in the terminal amine.

Fig. 3 Temperature dependence of the Co–ligand bond distances.

with those literature values having two long axial Co–O/N bonds in the range 2.15–2.25 Å and three equatorial Co–ligand bonds significantly shorter, between 1.9–2.0 Å.

Thus, the molecular geometry unambiguously leads to a description of the compound as containing three Co(II), and it follows that the sq-ligand in this system is acting as an innocent ligand. Further details of the database mining are given in the ESI.†

As mentioned, the coordination geometry of the two peripheral Co atoms is trigonal bipyramidal, while the central Co2 is octahedrally coordinated. One way to quantify the degree of degeneracy is to monitor the deviation from ideal geometry, which is suitably done by the continuous shape measurement method (CShM).[53] For the three Co atoms in **1**, these numbers are 0.55, 0.54, and 0.79 for Co1, Co2, and Co3, respectively, for the appropriate geometrical shapes; that is, trigonal bipyramid (Co1 and Co3) and octahedron (Co2). This implies that the geometries are close to ideal.

The idealized d-orbital splitting for C_{3v} and O_h, in combination with the d^7 configuration on Co(II), leads in both situations to significant overlap between half-filled d-orbitals and the ligands. Slightly smaller overlaps are expected for Co1 and Co3 on account of the presence of two electrons in the d-orbitals in the xy-plane in the trigonal bipyramidal hs-d^7 state (one from each of d_{xy} and $d_{x^2-y^2}$) compared to 2.67 electrons in the same plane in the octahedral geometry (one from $d_{x^2-y^2}$ and on average 1.67 in the d_{xy} orbital, in the case of complete degeneracy of the t_{2g} orbitals). This reduced population should manifest itself as shorter bond distances in the former, as is indeed observed in the present analysis.

High pressure crystallography

A sample of **1** was loaded inside a diamond-anvil cell (DAC) using Fomblin Y® as the pressure-transmitting medium and the effect of pressure on the crystal structure was monitored. The anticipated response to pressurisation is a transformation into a phase where the interatomic distances are reduced, which for hs-Co(II) can be accomplished by changing to a low-spin configuration (as described above).

Firstly, Fig. 4 shows the pressure dependence of the unit cell volume. From this figure it is clear that a discontinuous change in the pressure happens near 2 GPa with a sudden increase in volume and change in slope. This behaviour is most likely caused by a phase transition. The P–V data was fitted with a Birch–Murnaghan equation of state (EoS) using EosFit[54] separately for pressure points P1b–P5b and P6b–P8b (see Fig. 4, and ESI† for details on the EoS fits). Two very different bulk moduli of 4 GPa and 15 GPa were found from the two pressure ranges P1b–P5b and P6b–P8b, respectively. Since the fits are based on only a few points the absolute values are perhaps not so reliable, particularly so for the high pressure regime above 2 GPa, but the differences are nevertheless significant. Values of bulk moduli of 3–15 GPa lie within the general range seen for molecular crystals.[55]

Apart from the change in volume, the unit cell parameters and the atomic coordinates show no indication of a phase
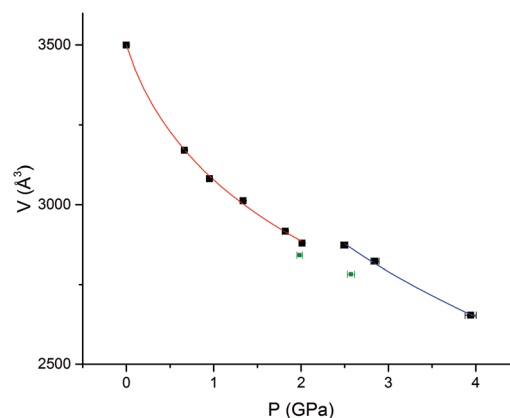

Fig. 4 Unit cell volume as a function of pressure. The black squares represent measured values while the lines mark an EoS fit of P1b–P5b (red) and P6b–P8b (blue). The green squares mark the volumes (divided by 2) of the new HP phase (P1–P2). See ESI† for more information on the EoS fits.

transition at 2 GPa. However, in another experiment, in which the pressure was increased immediately to 2 GPa, the unit cell volume was doubled while the space group type was unchanged. In this new phase, two independent molecules are now present, and the connectivity of one of these two is significantly changed compared to the low pressure polymorph (see Fig. 5a), while an overlay of the two independent molecules
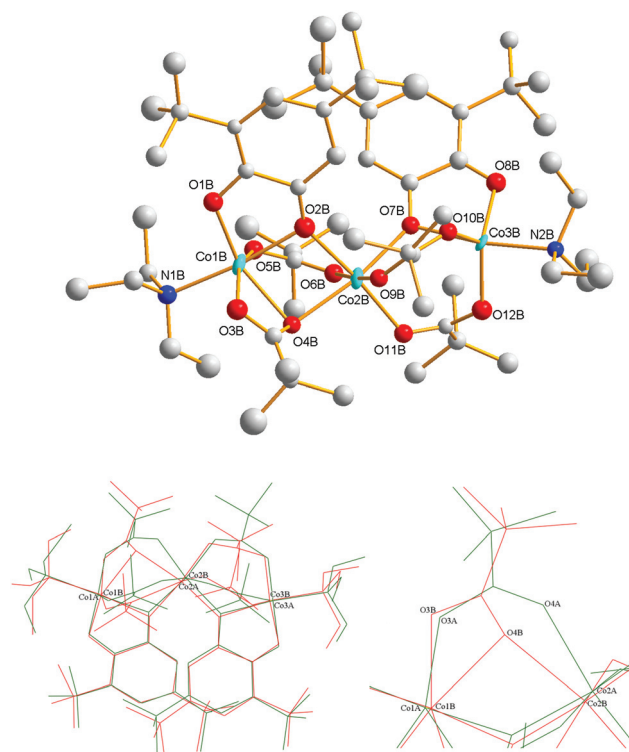

Fig. 5 (top) ORTEP drawing of the distorted molecule in the new HP phase; (bottom) overlay of the two independent molecules a (green) and b (red) in the compressed phase (left), with a zoom in on the changed coordination at the O3–O4 carboxylate bridge in molecule b (right).

clearly highlights these structural differences (see Fig. 5b). One of the two molecules (molecule a) is virtually unchanged, while in the other molecule (molecule b), one bridging carboxylate has changed coordination mode from $\mu_2:\kappa O:\kappa O'$ to $\mu_2:\kappa^2 O,O':\kappa O'$, with the consequence that the terminal Co1B is now closer to an octahedral coordination sphere, in contrast to its trigonal bipyramidal geometry at ambient pressure.

The Co–ligand bond distances in the high pressure phase indicate that no spin state change has taken place (see Table 1 and Fig. 6), although the bonds are all significantly shorter than at ambient geometry. It is noted that the most significantly changing bond distances are those from Co to the bridging oxygen from SQ (and also to the terminal amine, but due to the likely presence of disorder, this bond distance is not as reliable as the other distances). Another insight into the electronic structure of the compound may be obtained from the C–C and C–O bond distances in the SQ-based ligand. However, these cannot be obtained with sufficient precision from the HP data to allow an unambiguous determination of its oxidation state. Nevertheless, it is found that the C–O distances are virtually unchanged and the pattern of two shorter and four longer C–C bonds remain intact in the high pressure phase, indicating that the ligand still is a mono-anionic

semiquinonate, despite the changed connectivity in one of the two molecules.

Having established that the phase transition apparently is not accompanied by a change in the electronic structure, the question is why it happens. It may be imagined that it is related to the emergence of repulsive intermolecular interactions as the molecules approach, and to accommodate this energy penalty, one solution would be to rotate one of the pivalate groups thereby creating another Co–O interactions. A favourable method to examine whether this has happened is by Hirshfeld surface (HS) analysis. An analysis of the void spaces and HS were thus performed using the program Crystal Explorer.[56]

The analysis shows the expected trend of a decreasing void space within the crystal as the pressure is increased (see ESI†). The main contributor to the intermolecular interactions is H–H interactions with an average of 96.4% coverage of the HS (see ESI†), and these are also responsible for all the shortest contacts. However, as the structure is almost shrouded in a shell of H-atoms, this result is not surprising. There are no signs in the HS that the slow pressurisation from P1b to P3b leads to any significant repulsive interactions in the crystal structure, and the HS analysis therefore does not reveal the origin of the phase transition.

Magnetic properties

Variable temperature magnetic susceptibility measurements were employed to investigate the magnetic behaviour of **1** over the temperature range used for the structural studies. Fig. 7 plots $\chi_M T$ as a function of temperature under a static field of 0.1 T. The trace of $\chi_M T(T)$ decreases non-linearly as the temperature is reduced, reaching a value of 1.1 cm³ K mol⁻¹ at 8 K. This behaviour is likely due to two concurrent effects: (i) antiferromagnetic exchange interactions (either intra- or intermolecular) that favour a reduced total spin, and thus a decrease in magnetic susceptibility upon cooling; and (ii) the presence of ions with an unquenched orbital angular momentum, where the downward slope in the trace arises due to a

Table 1 Averaged Co–ligand bond distances for four different pressures. The (a) and (b) denotes the two independent molecules in the compressed phase. Subscripts t and c denote terminal and central Co, respectively. The μ_2-O atoms are O2 and O7, and in (b) also O4B. The other oxygens bonded to Co$_t$ are O1, O3, O5 for Co1 and O8, O10, O12 for Co3, and for Co$_c$ they are O4, O6, O9, O11

Pressure (GPa)	0	0.67	0.95	2.57 (a)	2.57 (b)
Co$_t$–(μ_2-O)	2.159	2.137	2.127	2.101	2.092
Co$_c$–(μ_2-O)	2.125	2.098	2.088	2.042	2.037
Co$_t$–O	1.974	1.968	1.960	1.941	2.027
Co$_c$–O	2.071	2.067	2.080	2.085	2.10
Co$_t$–N	2.216	2.192	2.166	2.138	2.124
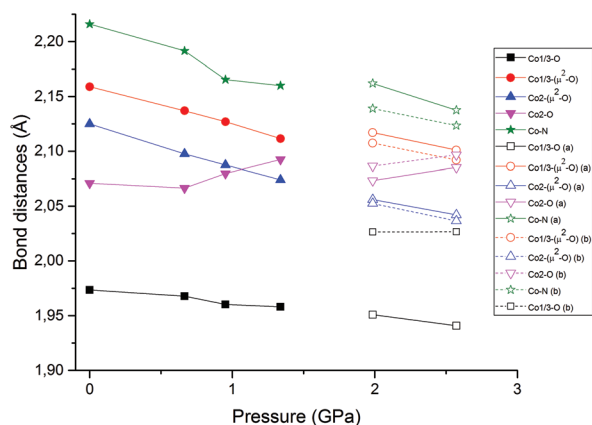
Fig. 6 Pressure dependence of the Co–O and Co–N bond distances. The filled symbols represent data from the first experiment (P0 and P1b–P3b), while the empty ones denotes the second experiment (P1–P2) with solid lines indicating molecule a and dashed lines for molecule b.
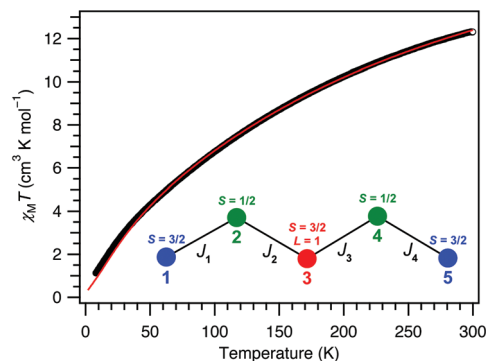
Fig. 7 Variable temperature magnetic susceptibility measured from 8–300 K. Experimental data are plotted in black circles with the simulation overlaid as a red trace. See main text for a full description of the model.

depopulation of the additional states generated by spin–orbit coupling interactions.

Given the minimum distance of 7.73 Å between paramagnetic centres in **1**, we neglect intermolecular exchange interactions entirely. Secondly, although the three cobalt centres are crystallographically independent, we choose to assume a pseudo symmetry that relates the two penta-coordinate centres, Co1 and Co3. This allows us to constrain the exchange interactions existing in each half of the molecule to be equivalent, while also setting the single ion properties of Co1 and Co3 to be identical. Thirdly, we assume isotropic g-values at all three cobalt centres, and we opt for purely isotropic exchange interactions (even though isotropic exchange is known to be a poor model for highly anisotropic ions in some cases[57]).

The octahedrally coordinated cobalt(II) ion (Co2), with ground term $^4T_{1g}$, is expected to possess a significant first-order orbital angular momentum, and this cannot be ignored. The intricate details governing the electronic properties of this ion are notoriously complicated, but in some cases a good approximation can be made using the T,P isomorphism, with an effective orbital moment, $\tilde{L} = 1$, and a coefficient of proportionality equal to $-3/2$.[58]

The single-ion anisotropy at the two penta-coordinate ions, with high-spin d^7 in a trigonal bipyramidal coordination environment, is less clear-cut. In a purely trigonal bipyramidal environment (D_{3h}), the ground term is $^4A'_2$, and hence there is no first-order orbital angular momentum. However, in a relatively weak crystal field, mixing in of excited terms with orbital momentum (*e.g. E* terms) would be expected to result in a small but significant contribution of orbital angular momentum to the ground state, which typically manifests as a zero-field splitting (ZFS). This is especially true when the coordination environment is distorted, as is the case in **1**. Despite this, we choose to assume spin-only behaviour in our initial attempts to model the data, since the ZFS parameter is expected to be heavily correlated with other parameters for susceptibility data, which are relatively insensitive to ZFS effects.

The appropriate Hamiltonian for the model described above is given in eqn (1).

Table 2 Parameters used for the simulation of $\chi_M T(T)$

Parameter	Value
g_1, g_2, g_4, g_5	2.0
g_3	5.67
J_1, J_4	$+36.5$ cm^{-1}
J_2, J_3	-221 cm^{-1}
λ	-170 cm^{-1}

We choose to fix $g_1 = g_2 = g_4 = g_5 = 2$, and we treat Co1 and Co3 as spin-only ions (*i.e.* $S_1 = S_5 = 3/2$, $L = 0$), for the reasons outlined above. The following parameters were allowed to refine freely during the least-squares regression fit: g_3, $J_1 = J_4$, $J_2 = J_3$. Table 2 lists all of the parameters in this model along with their final values after fitting to the experimental data using the program PHI,[59] and the simulated trace is overlaid on the data in Fig. 7.

Even with the various simplifying assumptions made during the modelling, we still run the risk of overparameterizing the model, and there is a strong likelihood of correlations between these three parameters; this is especially true of our data, which is largely featureless. In order to assess the extent of any correlations, we performed a survey of the residual as a function of all three fitted parameters. The results of this survey are shown in Fig. S9,† and indicate that although J_2 and g are correlated to some degree, our solution is the global minimum (see ESI†).

Overall, the model represents the experimental data very well, and at the very least supports the claim made during the structural analysis that all three Co-atoms in **1** remain in the *hs*-state over the entire temperature range. The absolute values from the simulation suggest a very strong anti-ferromagnetic coupling between the SQ radicals and the central octahedral Co(II), in accordance with previous results,[60,61] with a weaker ferromagnetic coupling between the five-coordinated Co and their nearest SQ radicals.

There are very few examples available in the scientific literature with which to compare our exchange model, which makes it difficult to provide context for the exchange parameters obtained here. In the few studies available, Co(II)-SQ exchange values range from $J = 0$,[62] to $J = -7$ cm^{-1},[13] to $J = -594$ cm^{-1},[63]

$$\hat{H} = \sum_{i=1}^{5}(-3/2\hat{l}_i + g_i\hat{s}_i)\beta\vec{H} - 2J_1(\hat{s}_1 \cdot \hat{s}_2 + \hat{s}_4 \cdot \hat{s}_5) - 2J_2(\hat{s}_2 \cdot \hat{s}_3 + \hat{s}_3 \cdot \hat{s}_4) + (-3/2)\lambda(\hat{l}_3 \cdot \hat{s}_3) \qquad (1)$$

The first term is the Zeeman interaction, the second and third terms are exchange interactions, and the final term represents the effective orbital approach described above, which attempts to account for the spin–orbit coupling on Co2 (site 3). A schematic is given in the inset of Fig. 7 that illustrates the connectivity in the model. Note that we are treating the semiquinonate moieties (sites 2 and 4) as $S = 1/2$ moieties in our model, and we are assuming that the superexchange pathway through the carboxylates is much smaller than that involving the semi-quinonates.

although it should be noted that the Hamiltonians used in the literature are not exactly the same in all cases.

As mentioned above, the model is based on a number of approximations, the most significant of which are the isotropy of the exchange interactions and the neglect of orbital contributions to the five-coordinate Co on site 1 and 5. The reliability of the absolute values depends heavily on the validity of these assumptions, and while the results from this work are closer to the calculated value from ref. 63, it is likely that more involved studies of **1** may lead to different absolute values.

Experimental

Synthesis

0.131 g (0.5 mmol) of $[Co(piv)_2]_n$ were dissolved in 9 mL of acetonitrile at room temperature. Under continuous stirring, a solution of 0.167 g (0.75 mmol) 3,5-di-*tert*-butylcatechol in 6 ml acetonitrile was added. The resulting dark solution was heated under reflux for ten minutes. After filtering off insoluble material, the solution was kept at 20 °C for 24 hours, after which 108 mg (0.09 mmol, 52.9%) of dark green crystals of complex **1** could be separated.

IR (KBr): ν (cm^{-1}) = 3434 (br), 2961 (s), 2866 (w), 1595 (s), 1481 (s), 1460 (m), 1412 (s), 1372 (m), 1227 (w), 1358 (m), 1096 (w), 1057 (w), 1028 (w), 987 (w), 892 (w), 867 (w), 787 (w), 740 (w), 610 (w), 582 (w), 427 (w). $C_{60}H_{106}Co_3N_2O_{12}$ (1223.7): calc. 58.86; H, 8.73; N, 2.29; exp. C, 58.61; H, 8.91; N, 2.28.

Ambient pressure X-ray crystallography

The crystallographic data for **1** are given below in Table 3. The X-ray data below 90 K were collected at beamline BL02B1 at SPring8 using a local He-cooling device. The diffractometer is equipped with a quarter-χ stage and the wavelength used for this experiment was 0.4997 Å. The data at 20 K was collected using a curved image-plate detector with automatic readout inside the hutch. The data at 40, 60, and 80 K were collected using a Rigaku CCD detector. The data were indexed, integrated and scaled using locally adapted Rigaku software based on the RAPID-AUTO suite of programs. The resulting Bragg intensities were averaged using SORTAV.[64,65]

The data at 90 K and above were collected using an Oxford Diffraction Supernova diffractometer equipped with a Mo microfocus source and an Atlas CCD detector. The crystal was cooled to the experimental temperature using an Oxford Cryosystems Cryostream 700 device. The data were collected using ω- and ϕ-scans, and final intensities for structure solution and refinement were obtained by integration, absorption-correction and merging using the CrysAlisPRO program. Selected crystallographic details for the 100 K data are given in Table 3, while full crystallographic tables can be found in the ESI.†

The structure was in all cases solved and refined using SHELXT[66] and SHELXL,[67] respectively, within the Olex2 package.[68]

High pressure crystallography

A suitable single crystal of dimensions 181 × 179 × ~50 µm was selected and mounted, and a data set at ambient pressure (P0) was collected. For the high pressure experiments, the crystal was loaded into a diamond anvil cell equipped with two Boehler-Almax anvils with 600 micron culets. The anvils were each seated on cubic boron nitride seats with 80 degree openings. A steel gasket was indented to a thickness of 108 microns and drilled with a hole of 300 microns. Fomblin Y cryoprotectant oil was used as the pressure transmitting medium. Two ruby spheres were loaded alongside the crystal of **1** to allow for pressure determination by monitoring of the R_1 fluorescence line of ruby. The DAC was mounted on a goniometer, and two high-pressure data sets were collected with pressures of 1.99 and 2.57 GPa, P1 and P2, respectively. As the phase transition had already taken place at P1 a new crystal with dimensions 200 × 94 × ~50 µm was mounted in the same DAC with the same gasket, now decreased to approximately 270 µm in diameter. Fomblin Y cryoprotectant oil was again used as pressure transmitting medium. Five new high-pressure data sets were collected, P1b–P5b, with pressures 0.67, 0.95, 1.34, 1.82 and 2.01 GPa. Further, three pre-experiments were run at higher pressures to determine only the unit cell parameters, not the crystal structure; 2.50, 2.85 and 3.94 GPa (P6b–P8b).

Magnetic susceptibility measurements

Magnetic susceptibility data were collected with a SQUID magnetometer (Quantum Design MPMS XL-7). The diamagnetic contribution of the sample was taken into account using Pascal constants. The temperature dependent magnetic contribution of the holder was experimentally determined and subtracted from the measured susceptibility data.

Conclusions

Detailed variable-temperature structural and magnetic studies of the first example of an oligomeric Co-dioxolene compound, $Co_3(piv)_4(SQ)_2(NEt_3)_2$ (**1**), unambiguously describes this compound as unable to engage in valence tautomerism in the studied temperature range from 8–200 K. The complex exhibits two types of Co-atoms exposed to significantly different ligand arrangements, with the central atom in a nearly octahedral geometry and the two others observing close to trigonal bipyramidal symmetry. The observed Co–ligand bond distances are

Table 3 Crystallographic data for **1** at 100 K

Formula	$C_{60}H_{106}Co_3O_{12}$
Molecular mass	1224.26
Space group	$P\bar{1}$
a (Å)	11.1736(3)
b (Å)	13.0734(4)
c (Å)	23.8027(7)
α (°)	85.002(2)
β (°)	80.744(2)
γ (°)	80.730(3)
V (Å^3)	3380.26(18)
Z	2
λ (Å)	0.71073
μ (mm^{-1})	0.782
T_{max}/T_{min}	1.000/0.8147
$F(000)$	1314
d_{min} (Å)	0.700
N_{meas}/N_{unique}	87 493/20 615
Redundancy	4.244
No. of parameters	862
R_{int}	0.049
Mean I/σ	14.4
Completeness	0.9998
GOF	1.053
$R_{all}(F)$	0.054
wR_2	0.097

explained in terms of d-orbital splitting schemes based on idealized symmetries. The structural description indicates high-spin states for all Co-sites, which is confirmed by a fit to the magnetic susceptibility data. A model ignoring magnetic anisotropy in the atomic parameters as well as in the exchange interaction, but explicitly including orbital contributions on the octahedral $Co(II)$ atom offers an exceptionally good description of the magnetic susceptibility. The derived values suggest a strongly anti-ferromagnetic coupling of -221 cm^{-1} between the central Co and the semi-quinone molecules, and quite strong anisotropy in the form of a g-value of 5.67.

It has previously been suggested that external pressure is able to initiate the VT transition, even in the case where temperature changes are ineffective. The reaction to the external pressure in **1** depends on the rate with which it was applied. This meant that a phase transition was induced if a pressure of 2 GPa was applied instantly, while if the pressure was increased slowly only subtle unit cell volume changes appeared leaving the crystal structure intact. The novel high pressure phase exhibited two independent molecules, of which one has a structure identical to the known at ambient pressure. In the other molecule, one bridging pivalato–ligand changes coordination mode to μ_2:κ^2O,O′:κO′ and the involved Co is closer to octahedral.

Analysis of the bond distances revealed that the high pressure crystal structure did not exhibit any changes in the spin and oxidation state of the Co-atoms nor the semiquinone ligands. Hirshfeld surface analysis was used to rule out the presence of strongly increased intermolecular repulsion with decreased intermolecular separation. The relatively small energy splitting of the d-orbitals due to the trigonal bipyramidal coordination of the two terminal Co-ions is speculated to be the main reason that no VT is observed for **1** in the given temperature and pressure range.

Acknowledgements

Notes and references

1 A. Calzolari, Y. Chen, G. F. Lewis, D. B. Dougherty, D. Shultz and M. Buongiorno Nardelli, *J. Phys. Chem. B*, 2012, **116**, 13141–13148.

2 A. Dei, D. Gatteschi, C. Sangregorio and L. Sorace, *Acc. Chem. Res.*, 2004, **37**, 827–835.

3 A. Witt, F. W. Heinemann and M. M. Khusniyarov, *Chem. Sci.*, 2015, **6**, 4599–4609.

4 V. I. Minkin, *Russ. Chem. Bull.*, 2009, **57**, 687–717.

5 J. Sedó, J. Saiz-Poseu, F. Busqué and D. Ruiz-Molina, *Adv. Mater.*, 2013, **25**, 653–701.

6 T. Tezgerevska, K. G. Alley and C. Boskovic, *Coord. Chem. Rev.*, 2014, **268**, 23–40.

7 C. G. Pierpont, *Coord. Chem. Rev.*, 2001, **216–217**, 99–125.

8 O.-S. Jung, D. H. Jo, Y.-A. Lee, Y. S. Sohn and C. G. Pierpont, *Angew. Chem., Int. Ed. Engl.*, 1996, **35**, 1694–1695.

9 R. M. Buchanan and C. G. Pierpont, *J. Am. Chem. Soc.*, 1980, **102**, 4951–4957.

10 O.-S. Jung and C. G. Pierpont, *Inorg. Chem.*, 1994, **33**, 2227–2235.

11 O. Cador, F. Chabre, A. Dei, C. Sangregorio, J. V. Slageren and M. G. F. Vaz, *Inorg. Chem.*, 2003, **42**, 6432–6440.

12 J. Tao, H. Maruyama and O. Sato, *J. Am. Chem. Soc.*, 2006, **128**, 1790–1791.

13 A. Witt, F. W. Heinemann, S. Sproules and M. M. Khusniyarov, *Chem. – Eur. J.*, 2014, **20**, 11149–11162.

14 O. Sato, A. Cui, R. Matsuda, J. Tao and S. Hayami, *Acc. Chem. Res.*, 2007, **40**, 361–369.

15 O. Sato, S. Hayami, Z.-Z. Gu, K. Takahashi, R. Nakajima, K. Seki and A. Fujishima, *J. Photochem. Photobiol., A*, 2002, **149**, 111–114.

16 O. Sato, S. Hayami, Z.-Z. Gu, K. Seki, R. Nakajima and A. Fujishima, *Chem. Lett.*, 2001, **30**, 874–875.

17 G. Poneti, M. Mannini, L. Sorace, P. Sainctavit, M.-A. Arrio, E. Otero, J. Criginski Cezar and A. Dei, *Angew. Chem., Int. Ed.*, 2010, **49**, 1954–1957.

18 A. Bencini, A. Caneschi, C. Carbonera, A. Dei, D. Gatteschi, R. Righini, C. Sangregorio and J. V. Slageren, *J. Mol. Struct.*, 2003, **656**, 141–154.

19 C. Roux, D. M. Adams, J. P. Itié, A. Polian, D. N. Hendrickson and M. Verdaguer, *Inorg. Chem.*, 1996, **35**, 2846–2852.

20 A. Caneschi, A. Dei, F. Fabrizi de Biani, P. Gütlich, V. Ksenofontov, G. Levchenko, A. Hoefer and F. Renz, *Chem. – Eur. J.*, 2001, **7**, 3926–3930.

21 B. Li, F.-L. Yang, J. Tao, O. Sato, R.-B. Huang and L.-S. Zheng, *Chem. Commun.*, 2008, 6019–6021, DOI: 10.1039/B814944E.

22 A. Beni, A. Dei, S. Laschi, M. Rizzitano and L. Sorace, *Chem. – Eur. J.*, 2008, **14**, 1804–1813.

23 Y. Mulyana, G. Poneti, B. Moubaraki, K. S. Murray, B. F. Abrahams, L. Sorace and C. Boskovic, *Dalton Trans.*, 2010, **39**, 4757–4767.

24 I. N. Markevtsev, M. P. Monakhov, V. V. Platonov, A. S. Mischenko, A. K. Zvezdin, M. P. Bubnov, G. A. Abakumov and V. K. Cherkasov, *J. Magn. Magn. Mater.*, 2006, **300**, e407–e410.

25 A. Droghetti and S. Sanvito, *Phys. Rev. Lett.*, 2011, **107**, 047201.

26 V. R. Hathwar, M. Stingaciu, B. Richter, J. Overgaard and B. B. Iversen, *Acta Crystallogr., Sect. B.*, 2016, submitted.

27 C. G. Pierpont and S. Kitagawa, in *Inorganic Chromotropism: Basic Concepts and Applications of Colored Materials*, ed. Y. Fukuda, Elsevier, Tokyo, 1st edn, 2007, pp. 116–142.

28 R. D. Schmidt, D. A. Shultz, J. D. Martin and P. D. Boyle, *J. Am. Chem. Soc.*, 2010, **132**, 6261–6273.

29 R. D. Schmidt, D. A. Shultz and J. D. Martin, *Inorg. Chem.*, 2010, **49**, 3162–3168.

30 O.-S. Jung, D. H. Jo, Y.-A. Lee, B. J. Conklin and C. G. Pierpont, *Inorg. Chem.*, 1997, **36**, 19–24.

31 V. I. Minkin, A. A. Starikova and A. G. Starikov, *Dalton Trans.*, 2015, **44**, 1982–1991.

32 C. Boskovic, in *Spin-Crossover Materials: Properties and Applications*, ed. M. A. Halcrow, Wiley, 2013, ch. 7, pp. 203–224.

33 H. Liang, Y. M. Na, I. S. Chun, S. S. Kwon, Y.-A. Lee and O.-S. Jung, *Bull. Chem. Soc. Jpn.*, 2007, **80**, 916–921.

34 M. P. Bubnov, N. A. Skorodumova, A. A. Zolotukhin, A. V. Arapova, E. V. Baranov, A. Stritt, A. Ünal, A. Grohmann, F. W. Heinemann, A. S. Bogomyakov, N. A. N. Smirnova, V. K. Cherkasov and G. A. Abakumov, *Z. Anorg. Allg. Chem.*, 2014, **640**, 2177–2182.

35 S. Bin-Salamon, S. H. Brewer, E. C. Depperman, S. Franzen, J. W. Kampf, M. L. Kirk, R. K. Kumar, S. Lappi, K. Peariso, K. E. Preuss and D. A. Shultz, *Inorg. Chem.*, 2006, **45**, 4461–4467.

36 Y. Teki, M. Shirokoshi, S. Kanegawa and O. Sato, *Eur. J. Inorg. Chem.*, 2011, **2011**, 3761–3767.

37 C. Carbonera, A. Dei, J.-F. Létard, C. Sangregorio and L. Sorace, *Angew. Chem., Int. Ed.*, 2004, **43**, 3136–3138.

38 B. Li, J. Tao, H.-L. Sun, O. Sato, R.-B. Huang and L.-S. Zheng, *Chem. Commun.*, 2008, 2269–2271, DOI: 10.1039/B801171K.

39 L. Chen, R. Wei, J. Tao, R. Huang and L. Zheng, *Sci. China: Chem.*, 2012, **55**, 1037–1041.

40 I. Imaz, D. Maspoch, C. Rodríguez-Blanco, J. M. Pérez-Falcón, J. Campo and D. Ruiz-Molina, *Angew. Chem., Int. Ed.*, 2008, **120**, 1883–1886.

41 X.-Y. Chen, R.-J. Wei, L.-S. Zheng and J. Tao, *Inorg. Chem.*, 2014, **53**, 13212–13219.

42 A. Beni, C. Carbonera, A. Dei, J.-F. Létard, R. Righini, C. Sangregorio and L. Sorace, *J. Braz. Chem. Soc.*, 2006, **17**, 1522–1533.

43 A. Beni, A. Dei, D. A. Shultz and L. Sorace, *Chem. Phys. Lett.*, 2006, **428**, 400–404.

44 S. H. Bodnar, A. Caneschi, A. Dei, D. A. Shultz and L. Sorace, *Chem. Commun.*, 2001, 2150–2151.

45 M. Affronte, A. Beni, A. Dei and L. Sorace, *Dalton Trans.*, 2007, 5253–5259.

46 W.-Q. Cheng, G.-L. Li, R. Zhang, Z.-H. Ni, W.-F. Wang and O. Sato, *J. Mol. Struct.*, 2015, **1087**, 68–72.

47 R. M. Buchanan, B. J. Fitzgerald and C. G. Pierpont, *Inorg. Chem.*, 1979, **18**, 3439–3444.

48 M. M. Olmstead, P. P. Power, G. Speier and Z. Tyeklár, *Polyhedron*, 1988, **7**, 609–614.

49 R. A. Reynolds, W. O. Yu, W. R. Dunham and D. Coucouvanis, *Inorg. Chem.*, 1996, **35**, 2721–2722.

50 M. Hmadeh, Z. Lu, Z. Liu, F. Gándara, H. Furukawa, S. Wan, V. Augustyn, R. Chang, L. Liao, F. Zhou, E. Perre, V. Ozolins, K. Suenaga, X. Duan, B. Dunn, Y. Yamamto, O. Terasaki and O. M. Yaghi, *Chem. Mater.*, 2012, **24**, 3511–3513.

51 H.-C. Chang, N. Nishida and S. Kitagawa, *Chem. Lett.*, 2005, **34**, 402–403.

52 P. Coppens, *X-Ray Charge Densities and Chemical Bonding (International Union of Crystallography Texts on Crystallography)*, International Union of Crystallography, 1997.

53 D. Casanova, P. Alemany, J. M. Bofill and S. Alvarez, *Chem. – Eur. J.*, 2003, **9**, 1281–1295.

54 J. Gonzalez-Platas, M. Alvaro, F. Nestola and R. Angel, *J. Appl. Crystallogr.*, 2016, **49**, DOI: 10.1107/S1600576716008050.

55 A. A. Yakovenko, K. W. Chapman and G. J. Halder, *Acta Crystallogr., Sect. B: Struct. Sci.*, 2015, **71**, 252–257.

56 J. J. McKinnon, M. A. Spackman and A. S. Mitchell, *Acta Crystallogr., Sect. B*, 2004, **60**, 627–668.

57 O. Kahn, *Molecular Magnetism*, Wiley, 1993.

58 B. N. Figgis and M. A. Hitchman, *Ligand Field Theory and Its Applications*, Wiley-VCH, 1999.

59 N. F. Chilton, R. P. Anderson, L. D. Turner, A. Soncini and K. S. Murray, *J. Comput. Chem.*, 2013, **34**, 1164–1175.

60 A. Bencini, A. Beni, F. Costantino, A. Dei, D. Gatteschi and L. Sorace, *Dalton Trans.*, 2006, 722–729, DOI: 10.1039/B508769D.

61 A. Caneschi, A. Dei, D. Gatteschi and V. Tangoulis, *Inorg. Chem.*, 2002, **41**, 3508–3512.

62 N. A. Protasenko, A. I. Poddel'sky, A. S. Bogomyakov, N. V. Somov, G. A. Abakumov and V. K. Cherkasov, *Polyhedron*, 2013, **49**, 239–243.

63 D. M. Adams, L. Noodleman and D. N. Hendrickson, *Inorg. Chem.*, 1997, **36**, 3966–3984.

64 R. H. Blessing, *Crystallogr. Rev.*, 1987, **1**, 3–58.

65 R. H. Blessing and D. A. Langs, *J. Appl. Crystallogr.*, 1987, **20**, 427–428.

66 G. Sheldrick, *Acta Crystallogr., Sect. A: Fundam. Crystallogr.*, 2015, **71**, 3–8.

67 G. M. Sheldrick, *Acta Crystallogr., Sect. A: Fundam. Crystallogr.*, 2008, **64**, 112–122.

68 O. V. Dolomanov, L. J. Bourhis, R. J. Gildea, J. A. K. Howard and H. Puschmann, *J. Appl. Crystallogr.*, 2009, **42**, 339–341.